Microgravity Science and Technology (2023) 35:4
https://doi.org/10.1007/s12217-022-10025-w

RESEARCH

Coupling Enhancement Effect of the Magnetic Field and Wall Superheat on Boiling Heat Transfer Characteristics of Magnetic Nanofluid (MNF) under Reduced Gravity

Kaikai Guo[1] · Huixiong Li[2] · Yuan Feng[3] · Tai Wang[4] · Jianfu Zhao[5,6]

Received: 5 September 2022 / Accepted: 7 December 2022 / Published online: 21 January 2023

Abstract

How to reduce or even eliminate the influence of gravity on boiling heat transfer, how to restrain the emergence of abnormally large bubbles and how to prevent the large decrease of critical heat flux (CHF) are the key to enhancing boiling heat transfer under reduced gravity. Magnetic nanofluid (MNF) boiling is one of the effective methods to solve the above problem. Under reduced gravity, the wall superheat has a crucial influence on the dynamics of the bubbles and boiling heat transfer. However, it has been unsolved whether the application of an external magnetic field can enhance the influence of wall superheat on boiling thermal dynamics or not. Based on the author's previous research, the influence of wall superheat on the enhanced heat transfer of MNF boiling under reduced gravity is further studied by using the computational model of MNF boiling heat transfer under external magnetic field. In this paper, the phase interface dynamics evolution and heat transfer characteristics of MNF boiling under the dual influence of wall superheat and magnetic field are described for the first time. The results show that the application of the magnetic field retards the flow state development of MNF film boiling compared with the results without the magnetic field. As the wall superheat increases, whether magnetic field is applied or not, the heat flux enhancement ratio with respect to wall superheat of 2 K under the various gravity level is almost the same. The effect of the wall superheat on boiling heat transfer characteristics under reduced gravity is enhanced by the application of external magnetic field. When the magnetic field of H = 20 kA/m is applied and the wall superheat is 6 K, under the three gravity levels of $g/g_e = 1.0$, $g/g_e = 0.44$ and $g/g_e = 0.11$, the heat flux with respect to wall superheat of 2 K can be enhanced up to 22.7%, 53.9% and 150.1%, furthermore, the heat flux enhancement rate can be enhanced up to 10%, 18.7% and 12.6%, respectively.

Keywords Reduced gravity · Magnetic field · Magnetic nanofluid (MNF) · Boiling · Wall superheat

✉ Kaikai Guo
guokaikai@cardc.cn

✉ Huixiong Li
huixiong@mail.xjtu.edu.cn

[1] Facility Design & Instrumentation Institute, China Aerodynamics Research and Development Center, Mianyang 621000, China

[2] State Key Laboratory of Multiphase Flow in Power Engineering, Xi'an Jiaotong University, Xi'an 710049, China

[3] North Institute of Mechanical & Electrical Engineering, Xianyang 712099, China

[4] School of Energy Power and Mechanical Engineering, North China Electric Power University, Baoding 071003, People's Republic of China

[5] CAS Key Laboratory of Microgravity, Institute of Mechanics, Chinese Academy of Sciences (CAS), Beijing 100190, China

[6] School of Engineering Science, University of Chinese Academy of Sciences, Beijing 100190, China

Nomenclature

$\mathbf{B}$	Magnetic induction intensity, (T)
c	Volume fraction of the discrete phase
c_p	Specific heat, (J/kg·K)
d	Distance, (m)
e	Heat flux enhancement ratio
$\mathbf{F}_\sigma$	Surface tension, (N/m^2)
$\mathbf{F}_m$	Magnetic force, (N/m^2)
$\mathbf{g}$	Gravitational acceleration, (m/s^2)
$\mathbf{H}$	Magnetic field intensity, (A/m)
$H(\phi)$	Smooth Heaviside function
h_{lv}	Latent heat of vaporization, (J/kg)
$\dot{m}$	Mass transfer rate, (kg/m^3.s)
p	Pressure, (pa)
$\dot{\mathrm{q}}$	Heat flux that causes the phase change at the phase interface, (W/m^2)
T	Temperature, (℃)
$\mathbf{u}$	Velocity, (m/s)

Greek letters

β_T	Volume expansion coefficient
$\delta(\phi)$	Dirac delta function
η	Dynamic viscosity, (kg/m·s)
λ	Thermal conductivity, (W/m·K)
μ	Magnetic permeability, (H/m)
μ_0	Vacuum permeability, $\mu_0 = 4\pi \times 10^{-7}$ H/m
ρ	Density, (kg/m^3)
σ	Surface tension coefficient, (N/m)
Γ	Phase interface
ϕ	Level Set function
φ	Volume concentration of nanoparticles
χ	Magnetic susceptibility
ψ	Magnetic potential, (At)
Ω	Control volume unit

Subscripts

e	Earth
v	Discrete phase
l	Continuous phase
mix	Mixture phase
p	Magnetic nanoparticles
w	Wall

Acronym

MNF	Magnetic nanofluid

Introduction

Due to its high heat transfer rate and small temperature difference, boiling heat transfer is widely used in many fields such as heat dissipation of electronic devices, thermal management system, thermal engineering and aerospace (Kharangate and Mudawar 2017). With the development of space technology, especially the gradual completion of China's space station, boiling heat transfer under reduced gravity has been widely concerned and studied (Celata 2015). Due to the decrease or even loss of buoyancy, boiling heat transfer has its special bubble dynamic behavior and heat transfer characteristics under reduced gravity (Dhir et al. 2012). The bubble departure diameter is much larger than that under the earth's gravity, and the bubble departure time increases significantly. Large bubbles covering the heated surface are difficult to escape, resulting in early heat transfer deterioration. And the critical heat flux (CHF) is much lower than that under the earth's gravity (Xue et al. 2011; Zhao et al. 2011; Konishi and Mudawar 2015). Compared with the results under the earth's gravity, the abnormally large bubble size and the large reduction of CHF under reduced gravity make it difficult to realize the advantages of boiling enhanced heat transfer technology in future space systems (Celata 2015; Konishi and Mudawar 2015). Therefore, how to reduce or even eliminate the influence of gravity on boiling heat transfer, how to restrain the emergence of abnormally large bubbles and how to prevent the large decrease of CHF are the key to enhancing boiling heat transfer under reduced gravity.

To explore the measures to further improve the efficiency of boiling heat transfer under reduced gravity, over the years, many scholars have made many attempts, such as optimizing the structure of heated surfaces (Liu et al. 2020), microchannels (Huang et al. 2020), nanofluids (Kim et al. 2007), the applied electric field (Pandey et al. 2017), the applied magnetic field (Guo et al. 2019a) and surfactants (Premnath et al. 2018). Different implementation methods and application backgrounds of the above measures lead to different enhancement effects, which mainly depend on the corresponding enhanced heat transfer mechanism. Since the introduction of nanofluids in 1995, nanofluids have been applied in many thermal management fields (Bahiraei et al. 2022; Mazaheri et al. 2022; Sheikholeslami and Ebrahimpour 2022; Sheikholeslami et al. 2022; Hosseinzadeh et al. 2021; Rostami et al. 2022). Magnetic nanofluid (MNF) is one of the nanofluids. MNF is favored by more and more scholars because of its unique advantages and is regarded as a new type of intelligent fluid. MNF is a colloidal solution in which magnetic nanoparticles dependent on surfactants are stably suspended in the base solution which can be water, kerosene, Freon, etc. Because of its highly effective thermal conductivity and heat transfer characteristics controlled by the external magnetic field, MNF as the new type of heat transfer working medium has broad application prospects in the field of thermal engineering.

Applying a magnetic field is considered as an active boiling heat transfer method, which can be combined with a passive method of adding nanoparticles to the base fluid to obtain synergistic results. In recent years, some researchers have combined the advantages of MNF and boiling heat transfer technology to study the MNF boiling heat transfer characteristics under the external magnetic field, and many important achievements have been achieved (Özdemir et al. 2018; Lee et al. 2012; Karimi-Moghaddam et al. 2014; Abdollahi et al. 2017). In the author's previous studies (Guo et al. 2019a, b), the author first developed a computational model of MNF boiling heat transfer with the magnetic field and systematically studied the characteristics of MNF boiling heat transfer with a uniform magnetic field and a non-uniform magnetic field. The results showed that the application of the external magnetic field can significantly improve the MNF boiling heat transfer efficiency. The author's results have attracted the attention of some scholars, who have also carried out some relevant studies (Sedaghatkish et al. 2020; Zhu et al. 2020; Chang et al. 2022). Given the result that the external magnetic field can significantly enhance boiling heat transfer efficiency, the author further studied the MNF boiling heat transfer characteristics

and phase interface thermodynamics under different reduced gravity (Guo et al. 2021), and the results showed that the characteristics of MNF boiling heat transfer under reduced gravity were basically the same as those under the earth's gravity by applying the magnetic field, and the problem of significant decrease of heat flux under reduced gravity was solved.

However, the MNF boiling under reduced gravity involves the interaction among flow, heat and mass transfer, and interfacial transport, which is a multiphase thermal fluid problem under the coupling of multiple physical fields. It is necessary to further study the mechanism of the MNF boiling heat transfer and explore innovative methods to improve the boiling heat transfer efficiency under reduced gravity. The previous studies (Wan and Zhao 2008; Ohta and Baba 2013; Ma et al. 2017) showed that the wall superheat had a crucial influence on the thermodynamic characteristic of boiling bubbles under reduced gravity, including bubbles growth and detachment, and heat transfer characteristics. With the continuous development of space technology, the heat of space equipment is getting higher and higher. Excessive wall superheat will seriously affect the safe operation of equipment. It is very important to clarify the boiling heat transfer of MNF in the reduced gravity under different wall superheat. There are many studies on the influence of wall superheat on boiling heat transfer of water, nanofluids, refrigerants and other media in the reduced gravity, but there are few studies on MNF. Furthermore, there are no reports on the phase interface dynamics evolution and heat transfer characteristics of MNF under the dual influence of the magnetic field and wall superheat in the reduced gravity. It remains to be studied whether applying an external magnetic field can enhance the effect of wall superheat on boiling thermodynamics or not. Based on the author's previous work, the influence of wall superheat on the heat transfer characteristics of MNF boiling under reduced gravity is studied in this paper. Firstly, we present the numerical methods used in our study. Secondly, the coupling effect of wall superheat and magnetic field is comprehensively expounded in terms of phase interface evolution and heat transfer characteristics. Finally, some conclusions are made.

Numerical Modelling

Governing Equations

The governing equations for viscous incompressible two-phase flow of MNF boiling with the magnetic field can be described as follows:

$$\frac{\partial c}{\partial t} + \mathbf{u} \cdot \nabla c = \frac{\dot{m}}{\rho_v} \tag{1}$$

$$\nabla \cdot (\mu \nabla \psi) = 0 \tag{2}$$

$$\nabla \cdot \mathbf{u} = \dot{m}\left(\frac{1}{\rho_v} - \frac{1}{\rho_l}\right) \tag{3}$$

$$\begin{aligned}\rho\left(\frac{\partial \mathbf{u}}{\partial \mathrm{t}} + \mathbf{u} \cdot \nabla \mathbf{u}\right) &= -\nabla p + \nabla \cdot \left[\eta\left((\nabla \mathbf{u}) + (\nabla \mathbf{u})^{\mathrm{T}}\right)\right] \\ &+ \rho \mathbf{g}\left(1 - \beta_T\left(T - T_{sat}\right)\right) + \mathbf{F}_\sigma + \mathbf{F}_m\end{aligned} \tag{4}$$

$$\frac{\partial T}{\partial t} + \mathbf{u} \cdot \nabla T = \frac{\lambda}{\rho c_p} \nabla^2 T \tag{5}$$

where, ρ, c, $\mathbf{u}$, p, η, $\mathbf{g}$, T, λ and c_p represent the density, the volume fraction of the dispersed phase, velocity, pressure, viscosity, gravitational acceleration, temperature, thermal conductivity, and specific heat, respectively. μ is relative permeability. Ψ is the scalar magnetic potential. $\dot{m}$ is the mass transfer rate. β_T is the coefficient of volumetric expansion. T_{sat} is the saturation temperature of the liquid phase. $\mathbf{F}_m$ represents the magnetic force. Detailed solving process of the above equations can be found in references (Guo et al. 2019a, 2021).

Phase Change Model

Ω represents the control volume unit and Γ is the phase interface, satisfying the following expression:

$$\int_{\Omega} \dot{m} dV = \frac{1}{h_{lv}} \int_{\Gamma} \dot{q} dA \tag{6}$$

where, h_{lv} is the latent heat of vaporization. $\dot{\mathrm{q}}$ is the heat flux that causes the phase change at the phase interface, and its expression is:

$$\dot{q} = \lambda_v \frac{\partial T}{\partial n}\bigg|_v - \lambda_l \frac{\partial T}{\partial n}\bigg|_l \tag{7}$$

Equation (6) establishes the relationship between the temperature field and the phase change rate $\dot{\mathrm{m}}$, also known as the Stefan condition at the phase interface. Thus, the solution of the phase change rate $\dot{\mathrm{m}}$ is transformed into the solution of the temperature gradient at both sides of the phase interface. For the temperature gradient on both sides of the phase interface, the normal probe technique proposed by Udaykumar (Udaykumar et al. 1999) and the bilinear interpolation method are used for calculation in this paper. Figure 1 shows the schematic diagram of the calculation method. The temperature gradient on both sides of the phase interface is as follows:

$$\frac{\partial T}{\partial n}\bigg|_v \approx \frac{-T_{A_2} + 4T_{A_1} + 3T_{sat}}{2d} \tag{8}$$

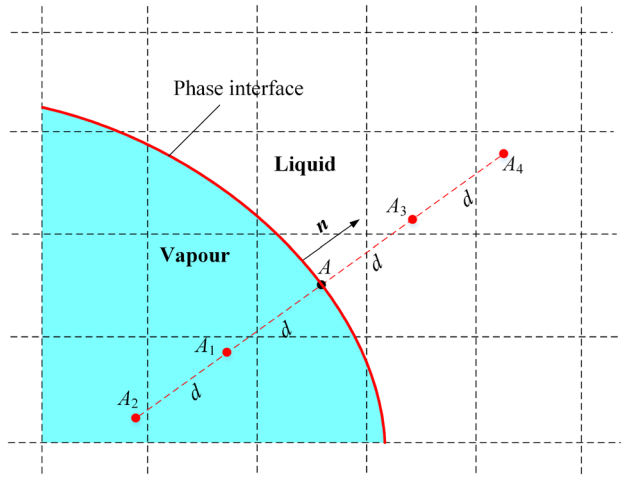

Fig. 1 Schematic of the normal probe technique

$$\left.\frac{\partial T}{\partial n}\right|_l \approx \frac{-T_{A_2} + 4T_{A_1} + 3T_{sat}}{2d} \tag{9}$$

In this paper, the processing method of (Ling et al. 2015) is adopted to solve the temperature of grid cells with phase interface. Figure 2 is taken as an example to introduce the solution process. For grid cells with phase interface, the temperature is calculated by linear interpolation along the normal direction of phase interface. If the grid center is located in the vapor phase, the interpolation point A' is found along the normal direction of the phase interface. The distance from point A' to the center point A of the grid is d. And then according to the distance between the center point A of the grid and phase interface $|\phi_A|$ to estimate the temperature T_A of center point A of the grid. If the center of the phase interface grid is in the liquid phase, the temperature T_B at the center of this cell can be calculated in the same way. The temperature of phase interface grids A and B can be calculated using the following formulas.

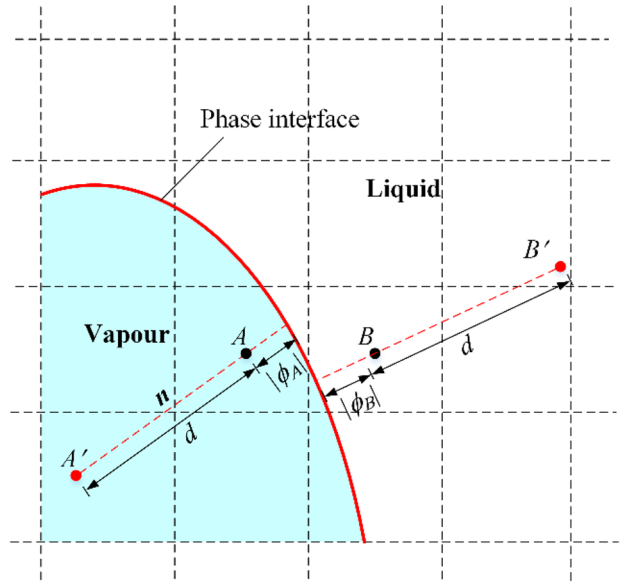

Fig. 2 Schematic of the solution method for the temperature at the center point of the cell containing the phase interface

Table 1 Properties of the MNF

	Liquid	Vapour	Nanoparticle
Density (kg/m^3)	200.0	5.0	5600.0
Thermal conductivity (W/m·K)	40.0	1.0	6.0
Thermal capacity (J/kg·K)	400.0	200	670.0
Dynamic viscosity (kg/m·s)	0.1	0.005	
Surface tension coefficient (N/m)	0.1		
Latent heat (J/kg)	10,000.0		
Magnetic susceptibility	0.2		

$$\frac{T_A - T_{sat}}{T_{A'} - T_{sat}} = \frac{|\phi_A|}{|\phi_A| + d} \tag{10}$$

$$\frac{T_B - T_{sat}}{T_{B'} - T_{sat}} = \frac{|\phi_B|}{|\phi_B| + d} \tag{11}$$

Physical Properties of the MNF

$$\text{Density}: \rho_{mix} = (1-\varphi)\rho_l + \varphi\rho_p \tag{12}$$

$$\text{Thermal capacity}: c_{p,mix} = \frac{(1-\varphi)\rho_l c_{p,l} + \varphi\rho_p c_{p,p}}{\rho_{mix}} \tag{13}$$

$$\text{Thermal conductivity}: \lambda_{mix} = \left(\frac{\lambda_p + 2\lambda_l - 2\varphi(\lambda_l - \lambda_p)}{\lambda_p + 2\lambda_l - \varphi(\lambda_l - \lambda_p)}\right)\lambda_l \tag{14}$$

$$\text{Dynamic viscosity}: \eta_{mix} = (1 + 2.5\varphi)\eta_l \tag{15}$$

where, φ is the volume concentration of MNF. The subscript p stands for magnetic nanoparticles.

Table 1 displays the physical properties of the MNF.

Magnetic Force Model

In the insulated MNF, there is no current or charge. The magnetic force comes from the interaction between the magnetic field and the magnetic dipole moment properties of each magnetic nanoparticle. In the case of MNF

two-phase flow, the permeability μ at the interface of two phase jumps and maxwell stress $\mathbf{T}_m$ is generated at the interface. The complete expression (Rosensweig 1985) of the magnetic force $\mathbf{F}_m$ is:

$$\mathbf{F}_m = \nabla \cdot \mathbf{T}_m = -\nabla\left[\mu_0 \int_0^{\mathrm{H}} \left(\frac{\partial M\upsilon}{\partial \upsilon}\right)_{H,T} dH + \frac{1}{2}\mu_0 H^2\right] + \mathrm{H}(\nabla \cdot \mathbf{B}) + \mathrm{B} \cdot \nabla \mathbf{H} \quad (16)$$

It is assumed that the magnetization M (μ, H, T) is a function of external magnetic field and temperature, and the MNF is the incompressible, isothermal linear magnetic material. By introducing the level set function ϕ, $\mathbf{F}_m$ can be ultimately simplified as:

$$\mathbf{F}_m = -\frac{1}{2}H^2\nabla\mu = -\frac{1}{2}H^2\left(\mu_c - \mu_d\right)\delta(\phi)\nabla\phi \quad (17)$$

Solution Method

In this paper, the computational model of MNF two-phase boiling with the magnetic field is implemented in the collocated grid system. Combined with a coupled volume-of-fluid and level set (VOSET) method (Sun and Tao 2010), the heat transfer characteristics and the thermodynamic characteristics of MNF boiling can be studied. The VOSET method not only has the advantages of the VOF

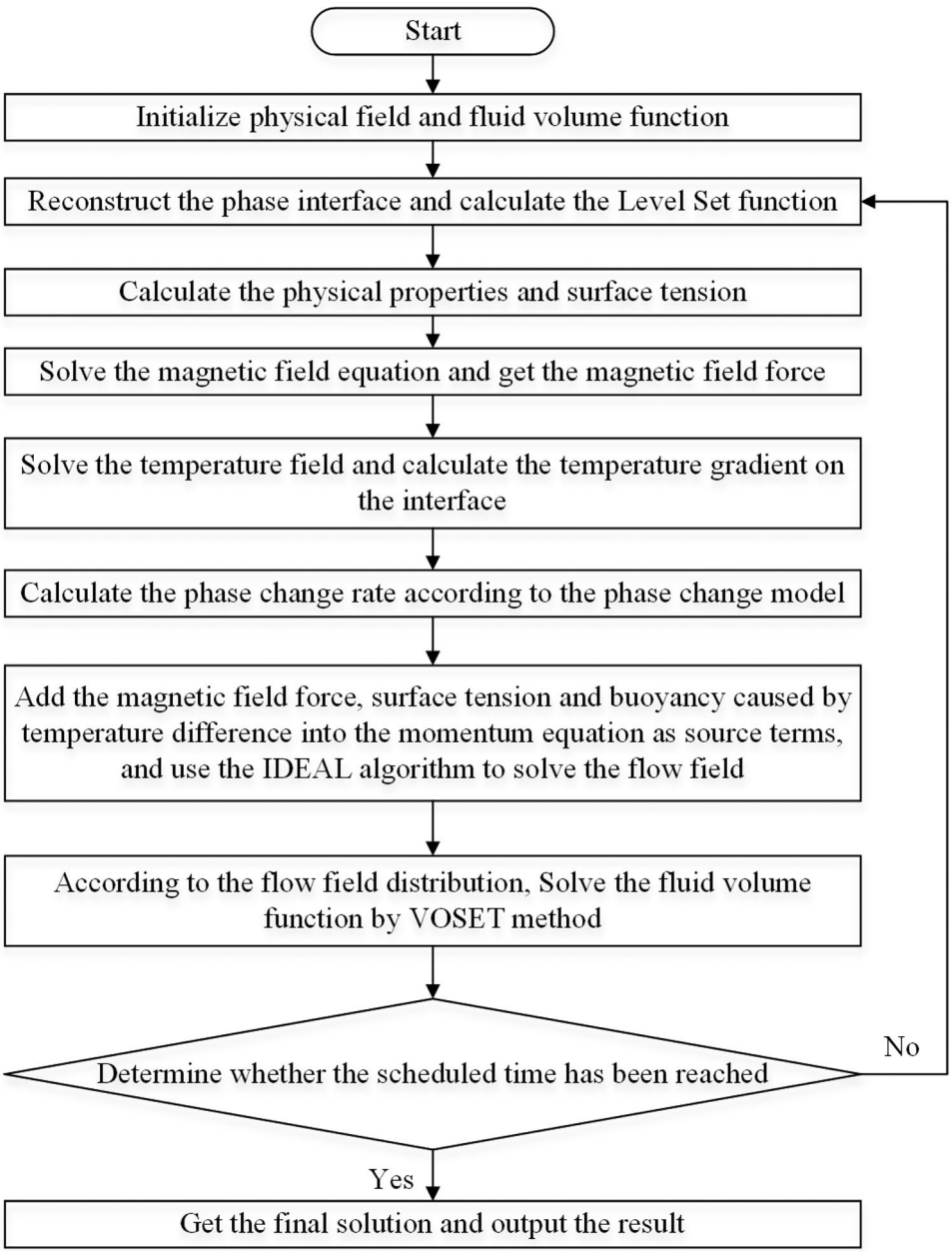

Fig. 3 Implementation process of the computational model of MNF boiling based on the VOSET method

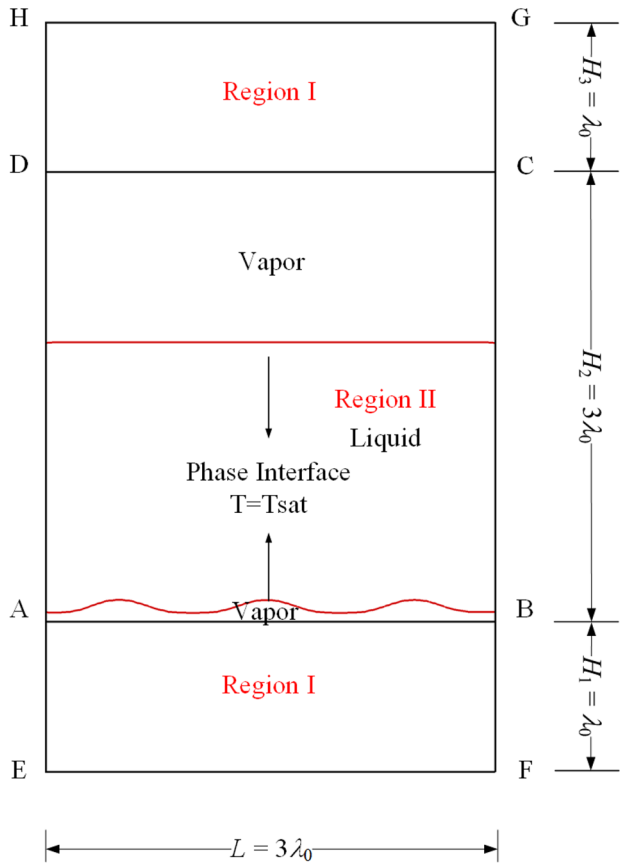

Fig. 4 Computational domain for the MNF film boiling simulation

method and Level Set method but also does not need to calculate the transport equation of the Level Set function and only needs to solve the VOF equation. Therefore, the calculation process of the VOSET method is more efficient. In this paper, the governing equations of the flow field, temperature field and magnetic field are discretized using a uniform structure grid. The QUICK scheme with high-order accuracy is used to discretize the convection term and the central difference scheme with second order accuracy is used to discretize the diffusion term. The unsteady IDEAL algorithm (Sun et al. 2008) is used to solve the flow field. Figure 3 shows the implementation process of the computational model of MNF boiling based on the VOSET method. The main steps are as follows:

The computational model of MNF boiling developed by the author has been verified in previous studies (Guo et al. 2019a, b), and has been used to research boiling heat transfer characteristics and thermodynamic characteristics of MNF under reduced gravity (Guo et al. 2021). Based on this work, the influence of wall superheat on boiling heat transfer characteristics of MNF under reduced gravity is further studied in this paper. Three gravity levels including earth's gravity g_e, $g/g_e = 0.44$, $g/g_e = 0.11$, as well as four wall superheat including 2 K, 4 K, 6 K and 8 K, are considered.

Computational Domain and Boundary Conditions

In the two-dimensional case, the Taylor instability wavelength λ_0 of film boiling is $\lambda_0 = 2\pi\sqrt{3\sigma/g(\rho_l - \rho_v)}$. To ensure that the fluid is in a uniform magnetic field and avoid the magnetic field boundary affecting the flow field, the computational region is divided into two regions. The magnetic field is solved in region **I** (EFGH), and the flow field is solved in region **II** (ABCD), as shown in Fig. 4. The computational domain for solving the magnetic field is chosen to be $3\lambda_0 \times 5\lambda_0$ and the computational domain for solving the flow field is chosen to be $3\lambda_0 \times 3\lambda_0$. According to the gas–liquid interface obtained from region **II**, region **I** is calculated until region **I** is stable, and region **I** and region **II** are simultaneously solved by a coupling iteration approach.

Symmetry conditions are provided at the left and right boundaries both regions **I** and **II** as

$$\begin{aligned} ABCD &: u = 0, \frac{\partial v}{\partial x} = 0, \frac{\partial T}{\partial x} = 0 \\ EFGH &: \frac{\partial \psi}{\partial x} = 0 \end{aligned} \tag{18}$$

The top wall of region **I** is explicitly defined at a constant magnetic field intensity and outflow condition is incorporated at the top boundary of region **II**. The conditions are mentioned as follows:

$$\begin{aligned} ABCD &: \frac{\partial u}{\partial y} = \frac{\partial v}{\partial y} = \frac{\partial T}{\partial y} \\ EFGH &: \frac{\partial \psi}{\partial y} = -\frac{\mu_0}{\mu_g} H_0 \end{aligned}, \tag{19}$$

The bottom wall of region **I** is explicitly defined at a constant magnetic field intensity. A no-slip wall condition is incorporated at the bottom boundary of region **II**. The conditions are defined as follows:

$$\begin{aligned} ABCD &: u = v = 0 \\ EFGH &: \frac{\partial \psi}{\partial y} = -\frac{\mu_0}{\mu_g} H_0 \end{aligned} \tag{20}$$

Details about the computational domain can be also found in references (Guo et al. 2019a, 2021).

Results and Discussion

Phase Interface Evolution

(a) Without the magnetic field

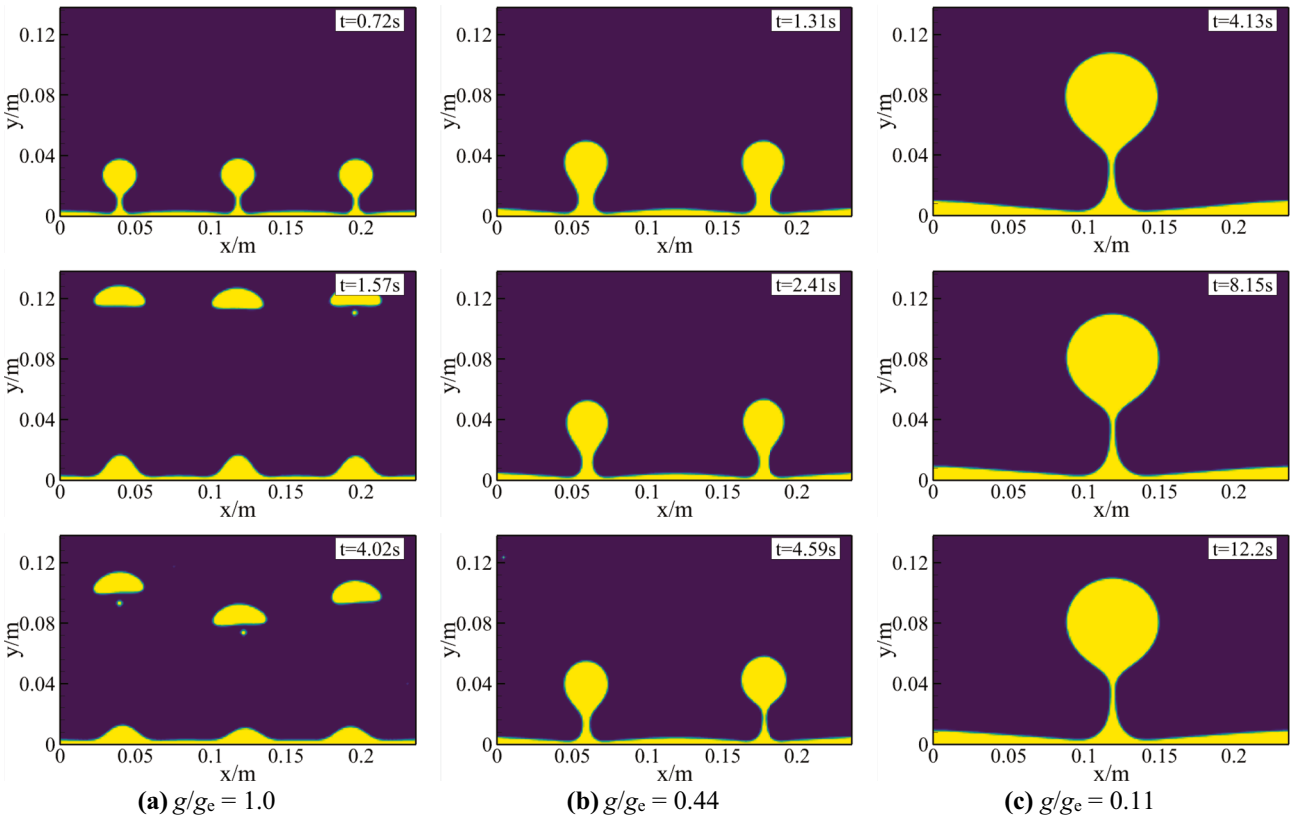

Fig. 5 Interface evolution with time for the wall superheat of 2 K

Figures 5, 6, 7 and 8 show the influence of wall superheat on the bubble detachment morphology under the three gravity levels ($g/g_e = 1.0$, $g/g_e = 0.44$ and $g/g_e = 0.11$), where g_e represents the earth's gravity of 9.81 N/kg. It can be seen that the evolutionary morphology of the bubble interface is very different under three gravity levels. Firstly, the evolution characteristics of the phase interface under the earth's gravity are analyzed. Under the earth's gravity, buoyancy dominates bubble detachment and the bubbles lift off easily. When the wall superheat is low (2 K), the growth and detachment of bubbles always present periodic characteristics, as shown in Fig. 5a. When the wall superheat increases to 4 K, more heat input lead to higher bubble detachment frequency and stronger instability of the bubble phase interface. The phase interface morphology changes and no longer has periodicity, as seen in Fig. 6a. At the initial stage, the growth and detachment process of bubbles is periodic, but after several bubbles break away, the flow state becomes disordered. Over time, bubbles begin to coalesce to form columns. With the heat transport on the wall, the vapor column is gradually extended. When it reaches a certain length and under a certain disturbance, the vapor column begins to break and form small bubbles and then detach. According to the above analysis, when the wall superheat is 4 K, the flow state is in the state of bubble flow and vapor column flow simultaneously. When the wall superheat further increased to 6 K, as shown in Fig. 7a, the flow state enters the simultaneous existence of bubble flow and column flow after the first few bubbles break away. When the wall superheat increased to 8 K, as shown in Fig. 8a, the simultaneous existence of bubble flow and column flow no longer appear. After the initial several bubbles break away, the flow state immediately changes to column flow, and the vapor column length gradually increases with the continuous input of heat.

The evolution of bubble interface under reduced gravity is very different from that under the earth's gravity. Under reduced gravity, buoyancy no longer dominates bubble detachment, the bubble becomes harder to depart. The unstable modes at the bubble interface require higher heat to excite. At the reduced gravity of $g/g_e = 0.44$, when the wall superheat is 2 K and 4 K, the growth and detachment of bubbles are periodic, as shown in Figs. 5b and 6b. This indicates that the wall superheat limit corresponding to the peri-

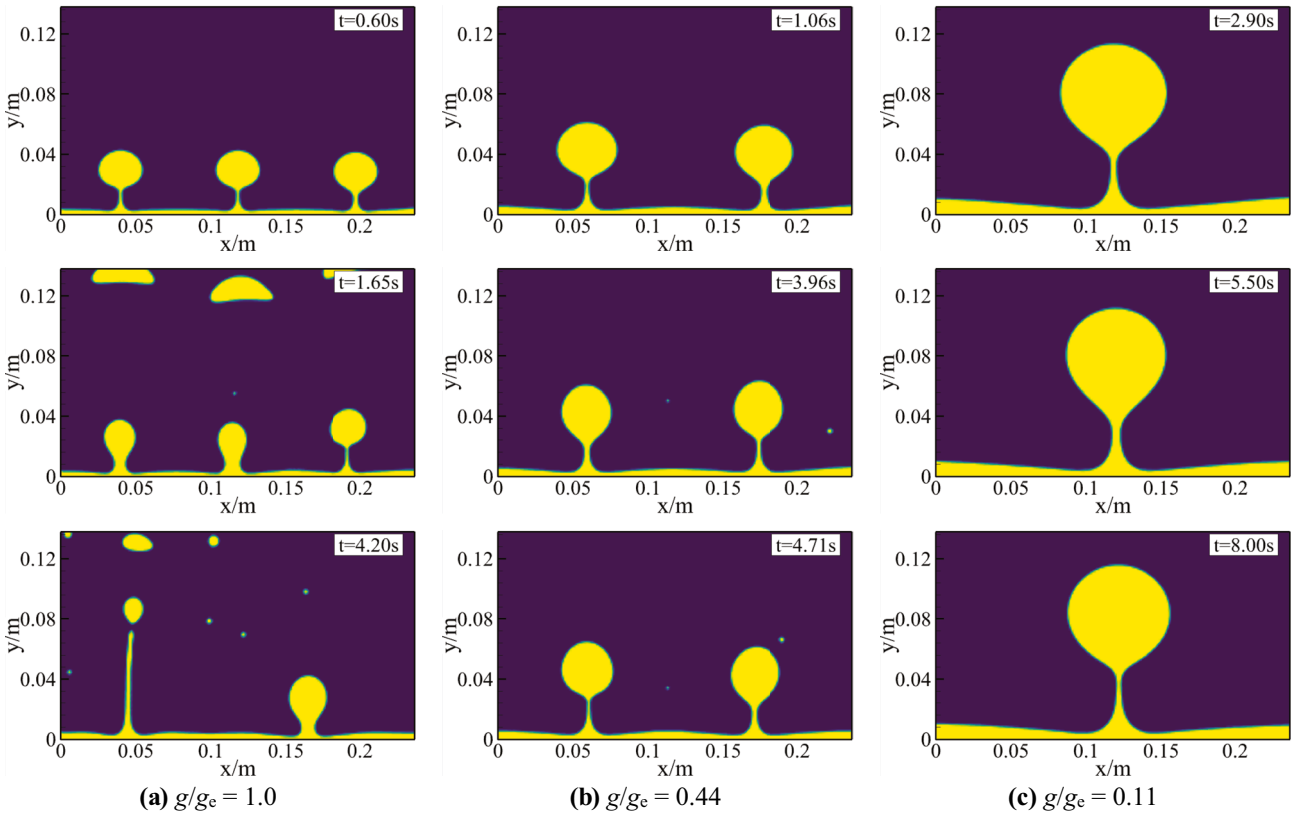

Fig. 6 Interface evolution with time for the wall superheat of 4 K

odic growth and detachment of bubbles increases from 2 to 4 K compared with the earth's gravity. When the wall superheat increases further, the growth and detachment of bubbles are still periodic in the initial period. When the wall superheat is 6 K and 8 K, the stability period is 5.5 s and 4.0 s, respectively. The larger the wall superheat is, the shorter the initial stability period is, as shown in Figs. 7b and 8b. When the initial stability time is exceeded, the growth and detachment of bubbles are no longer periodic and the flow pattern becomes disordered. However, the flow pattern is still in the bubble flow, there is no vapor column flow. When the gravity level is further reduced to $g/g_e = 0.11$, the phase interface morphology of the bubble is different from that of the first two gravity levels. When the wall superheat is in the range of 2 K ~ 8 K, the growth and detachment of bubbles are always periodic, as shown in Figs. 5c, 6c, 7c and 8c.

(b) With the magnetic field

Figures 9, 10, 11 and 12 show the evolutionary morphology of the vapor bubble in the wall superheat range of 2 K ~ 8 K under the vertical uniform magnetic field with $H = 20$ kA/m. It is obvious from the figures that the evolutionary morphology of the bubble with the magnetic field is very different from the result without the magnetic field. When the magnetic field is applied, the departure time and the departure diameter of separated bubbles are greatly reduced due to the existence of the magnetic field force. The magnetic field force causes the disturbance and deformation of the phase interface and then the dynamic characteristics of the phase interface affect the velocity field nearby. The larger the magnetic field intensity, the greater the magnetic field force acting on the bubble, leading to an increase in the departure time and the departure diameter (Guo et al. 2019b). When the magnetic field is applied and the wall superheat is 2 K and 4 K, the film boiling flow is in a disordered bubble flow under the earth's gravity. When the wall superheat increases to 6 K and 8 K, the flow state of film boiling changes to the state of both bubble flow and vapor column flow. The results show that the main reason causing the bubble to escape is that the phase interface is disturbed due to the presence of the magnetic field so the instability

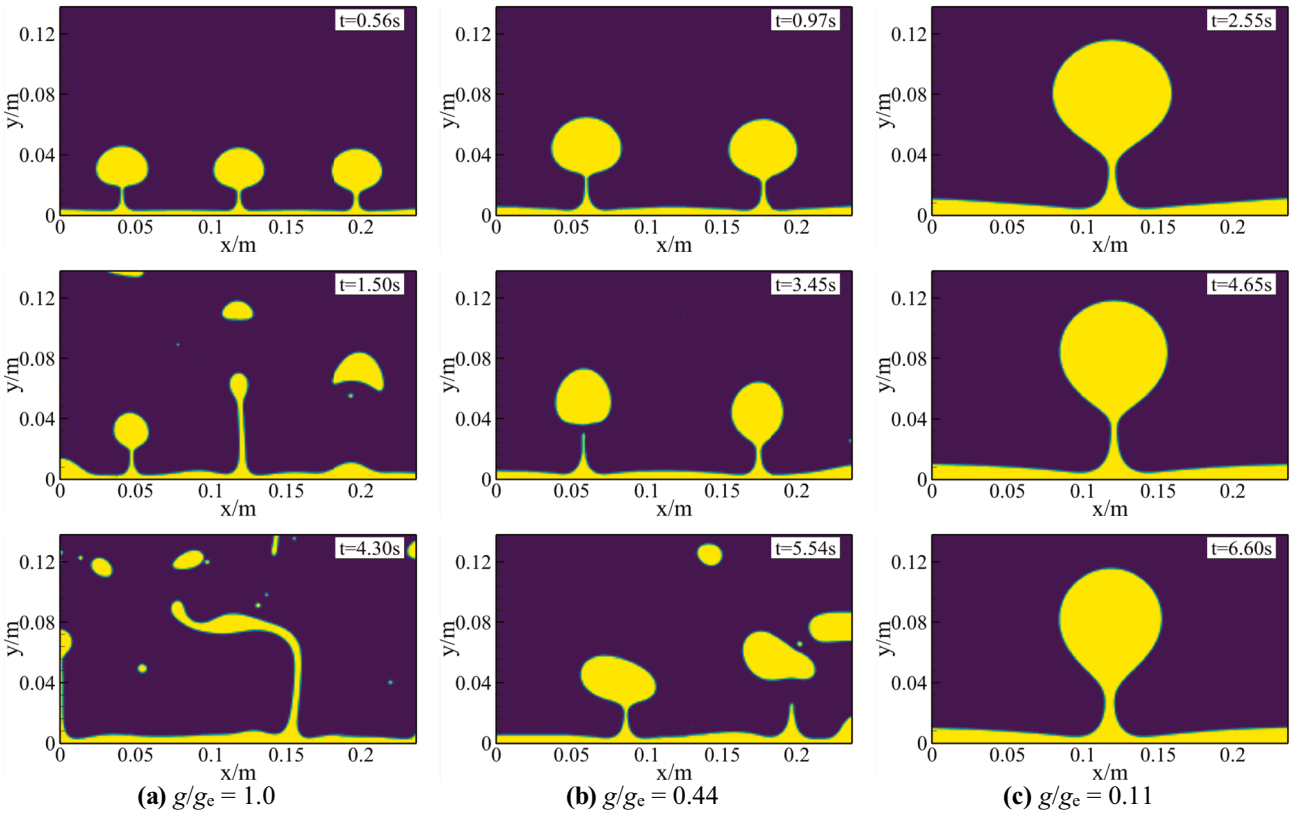

Fig. 7 Interface evolution with time for the wall superheat of 6 K

of the phase interface becomes more intense. Consequently, the more intense the phase interface, the easier it is for the bubble to escape. Compared with the results without the magnetic field, the applied magnetic field retards the development of film boiling flow. Under reduced gravity, the evolutionary morphology of the vapor bubble is very different from that without the magnetic field. In the absence of the magnetic field, under reduced gravity of $g/g_e = 0.44$, the film boiling flow in the wall superheat range of 2 K ~ 8 K is in the bubble flow with regular bubble departure. After applying a magnetic field, the film boiling flow becomes stable and regular vapor column flow. However, the stability of the vapor column flow becomes weaker with the increase of the wall superheat. When the gravity level decreases to $g/g_e = 0.11$, the film boiling flow is transformed into an unstable and irregular vapor column flow, and the instability and irregularity become more and more intense with the increase of the wall superheat.

Heat Transfer Characteristics

(a) Without the magnetic field

The spatial average heat flux can be defined as:

$$q_w = \frac{1}{X}\int_0^X q'_w dx \tag{21}$$

where X is the length in the x direction of the computational domain and q'_w is the local heat flux, which is written as:

$$q'_2 = \lambda_v \frac{\partial T}{\partial y}\bigg|_{v,y=0} \tag{22}$$

Figure 13 shows the variation of the spatial average heat flux of film boiling without the magnetic field. As shown in Fig. 13a, when the wall superheat is 2 K, the variation of the spatial average heat flux at the heated wall under three gravity levels all show periodicity. The distribution of heat flux can also explain

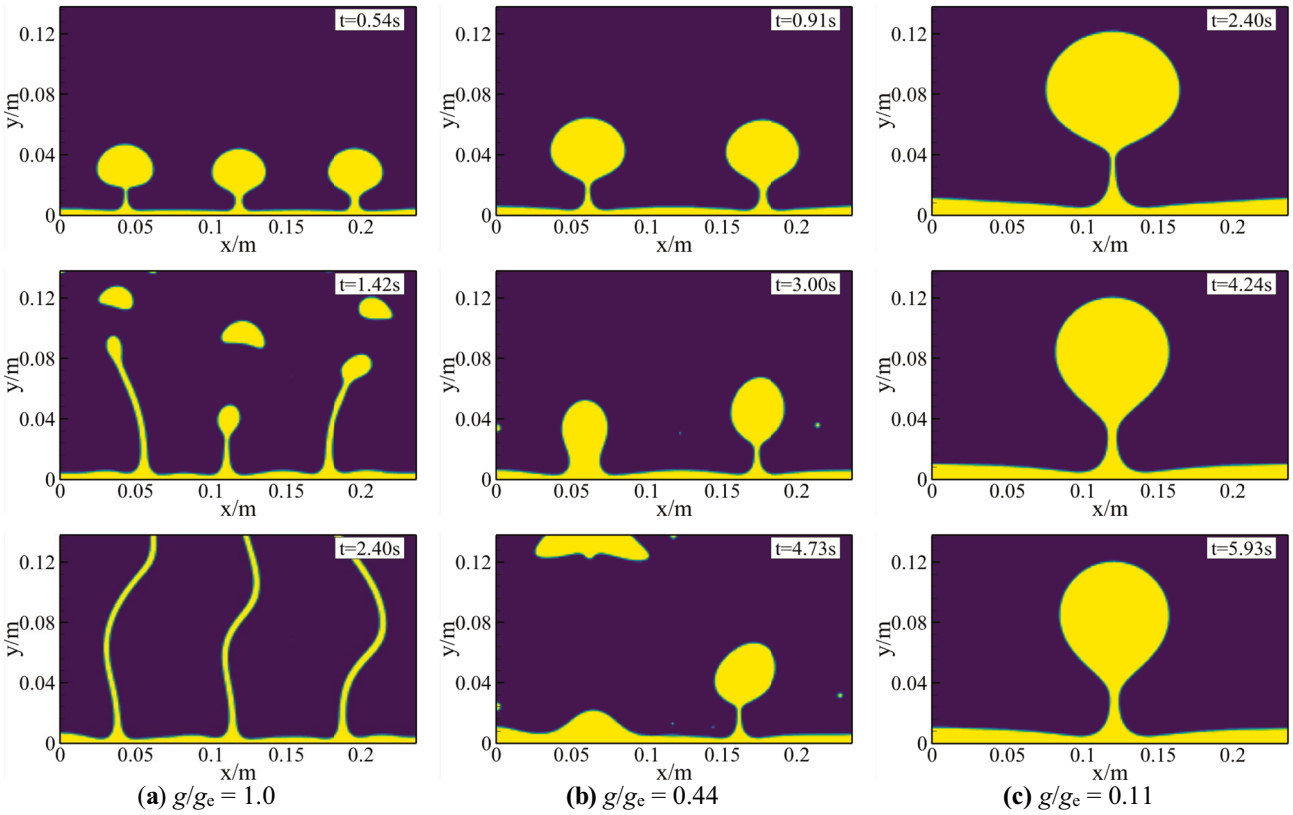

Fig. 8 Interface evolution with time for the wall superheat of 8 K

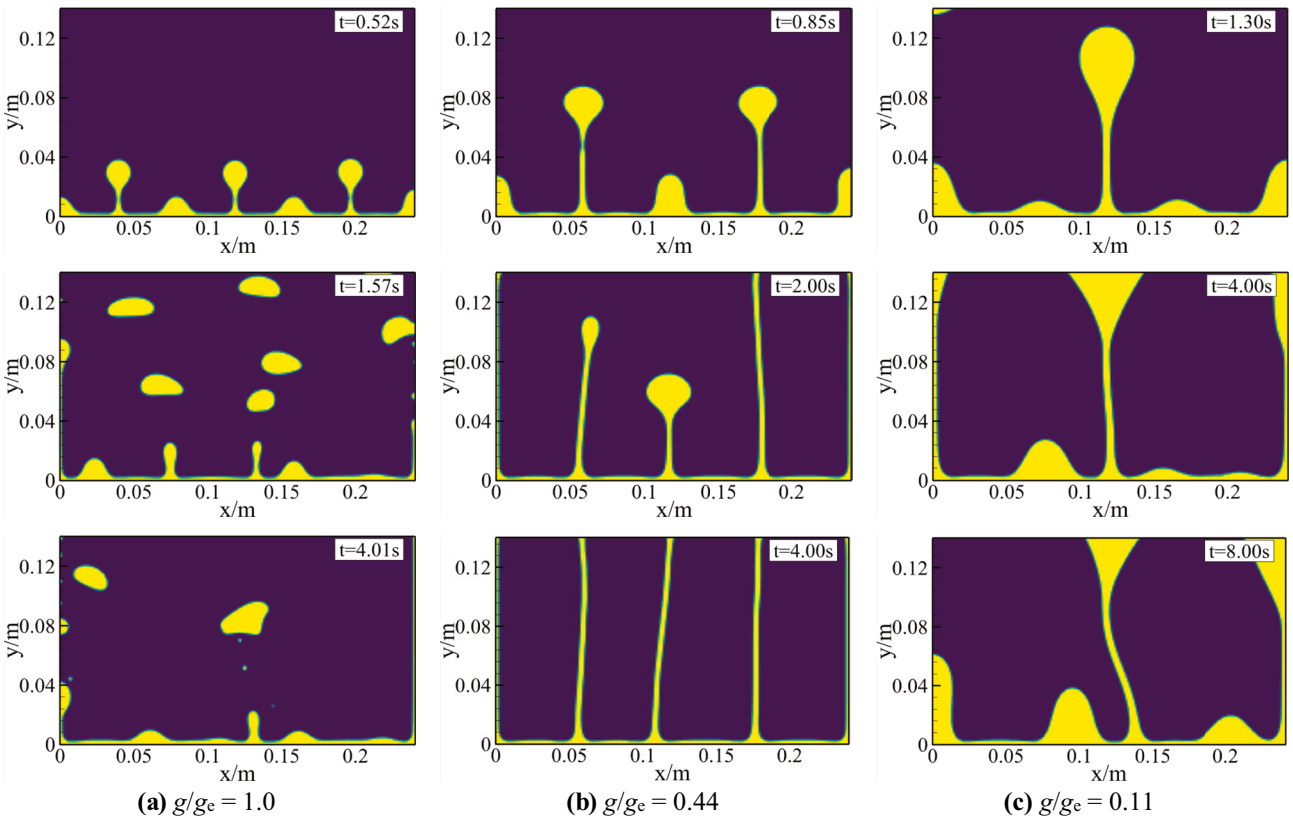

Fig. 9 Interface evolution for the wall superheat of 2 K and applied magnetic field of $H = 20$ kA·m.$^{-1}$

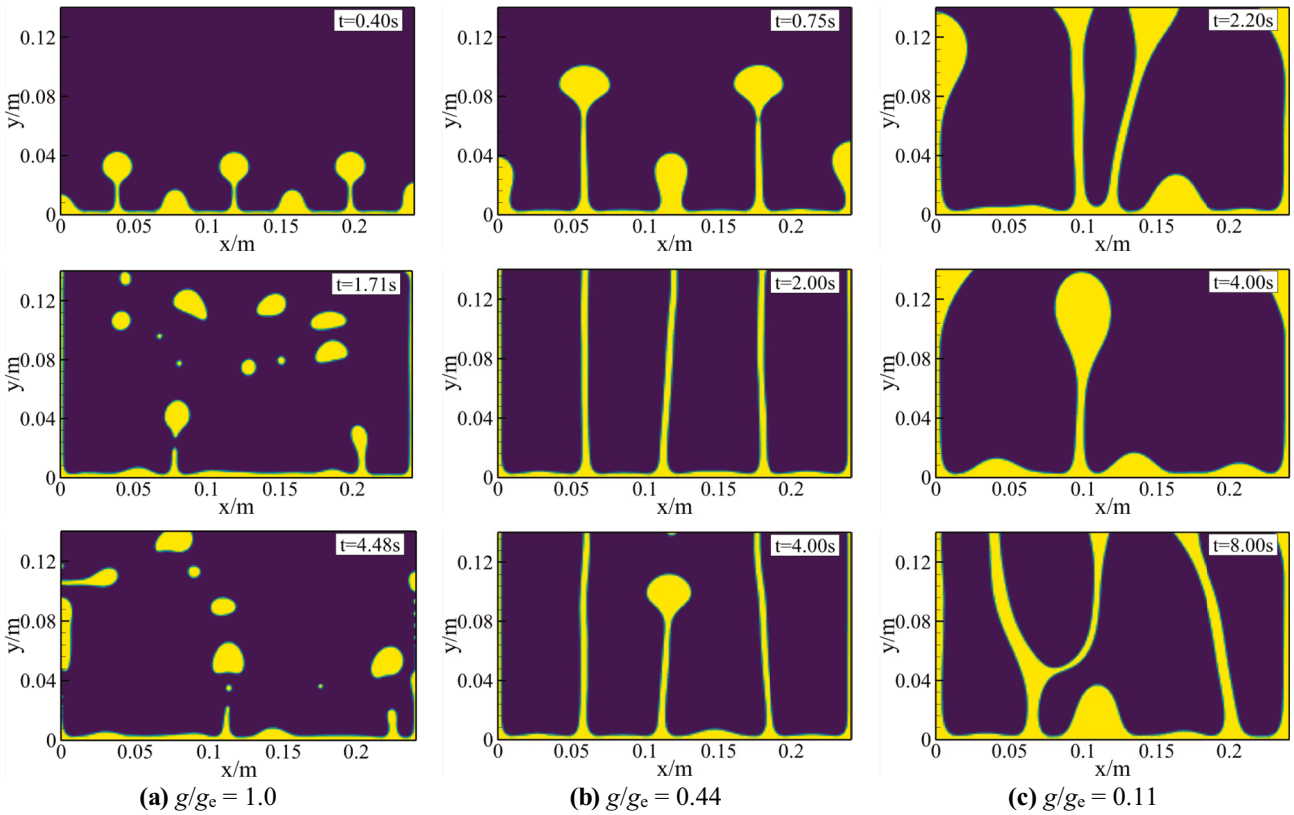

Fig. 10 Interface evolution for the wall superheat of 4 K and applied magnetic field of $H = 20$ kA/m

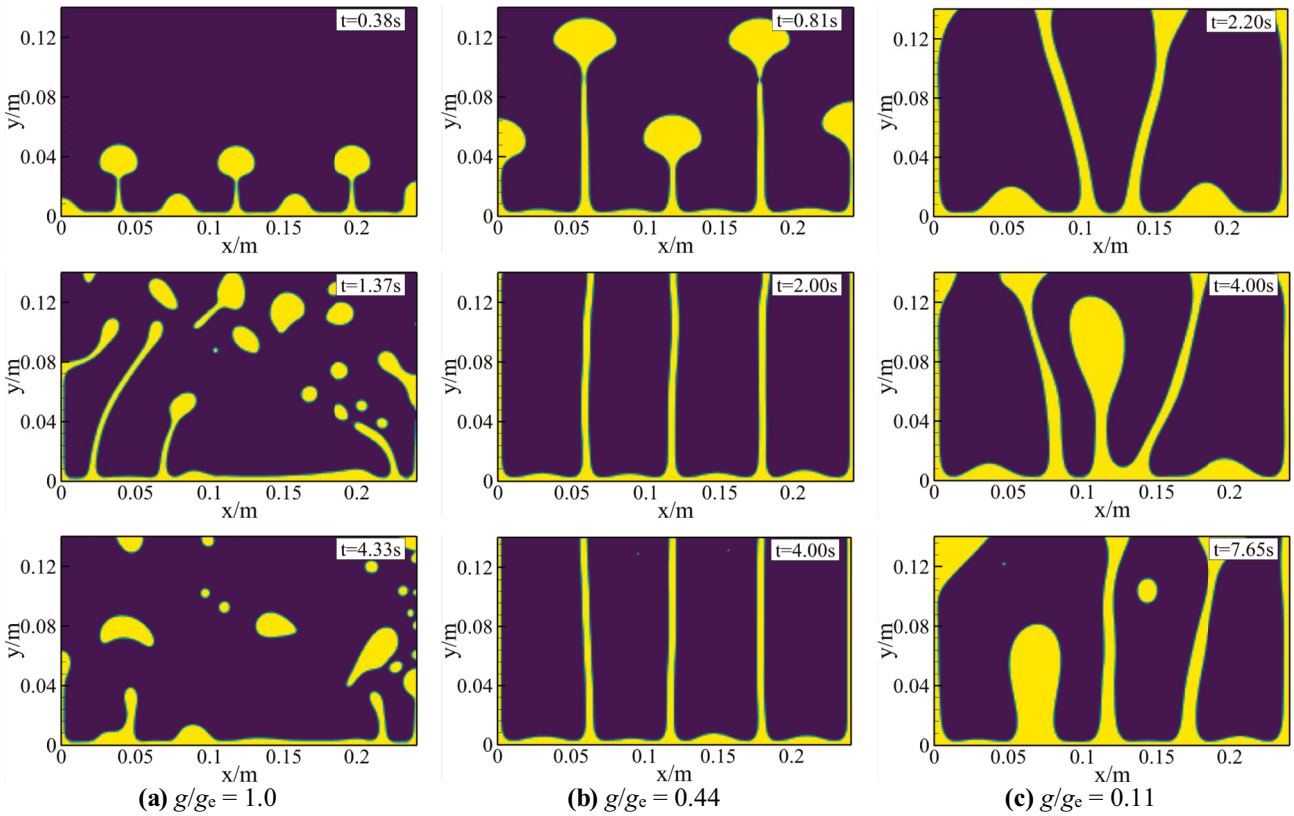

Fig. 11 Interface evolution for the wall superheat of 6 K and applied magnetic field of $H = 20$ kA/m

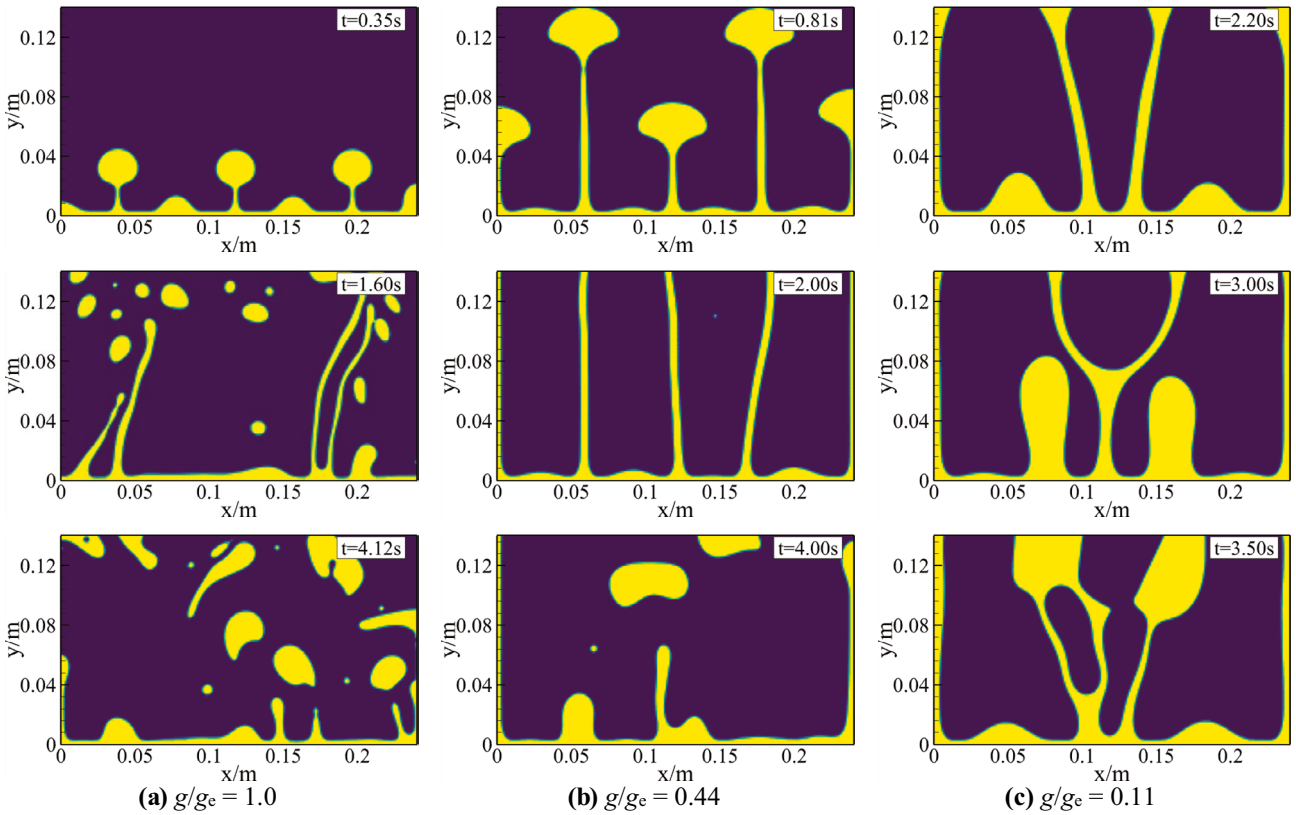

Fig. 12 Interface evolution for the wall superheat of 8 K and applied magnetic field of $H = 20$ kA/m

the growth and separation of bubbles. When the wall superheat increases to 4 K, the spatial average heat flux under the earth's gravity no longer exhibits periodicity, while the spatial average heat flux still exhibits periodicity under the other two gravity levels, as shown in Fig. 13b. When the wall superheat is further increased to 6 K, the spatial average heat flux under $g/g_e = 1.0$ and $g/g_e = 0.44$, no longer shows periodicity, as shown in Fig. 13c. Under $g/g_e = 1.0$, the curve of the spatial average heat flux is almost unchanged with time after t = 5.0 s, and it can be predicted that the vapor column flow has formed. Under $g/g_e = 0.44$, the spatial average heat flux changes periodically with time before t = 6.0 s, but after that, the amplitude of the curve of the spatial average heat flux with time decreases, indicating that the bubble detachment has become disordered. Under $g/g_e = 0.11$, the spatial average heat flux changes periodically with time. When the wall superheat continues to increase to 8 K, it can be seen from Fig. 13d that the formation of vapor column flow is advanced under $g/g_e = 1.0$. Under $g/g_e = 0.44$, the variation of spatial average heat flux with time is periodic before t = 4.0 s, but after that, the variation curve of spatial average heat flux with time becomes disordered. Under $g/g_e = 0.11$, the spatial average heat flux still shows periodicity with time.

The space- and time- averaged heat flux can be expressed as:

$$\overline{q_w} = \frac{1}{T}\int_0^T q_w dt \tag{23}$$

where T is the total computation time.

The heat flux enhancement ratio e represents the ratio of space- and time-averaged heat flux between other wall superheats and 2 K, which can be calculated by the following expression:

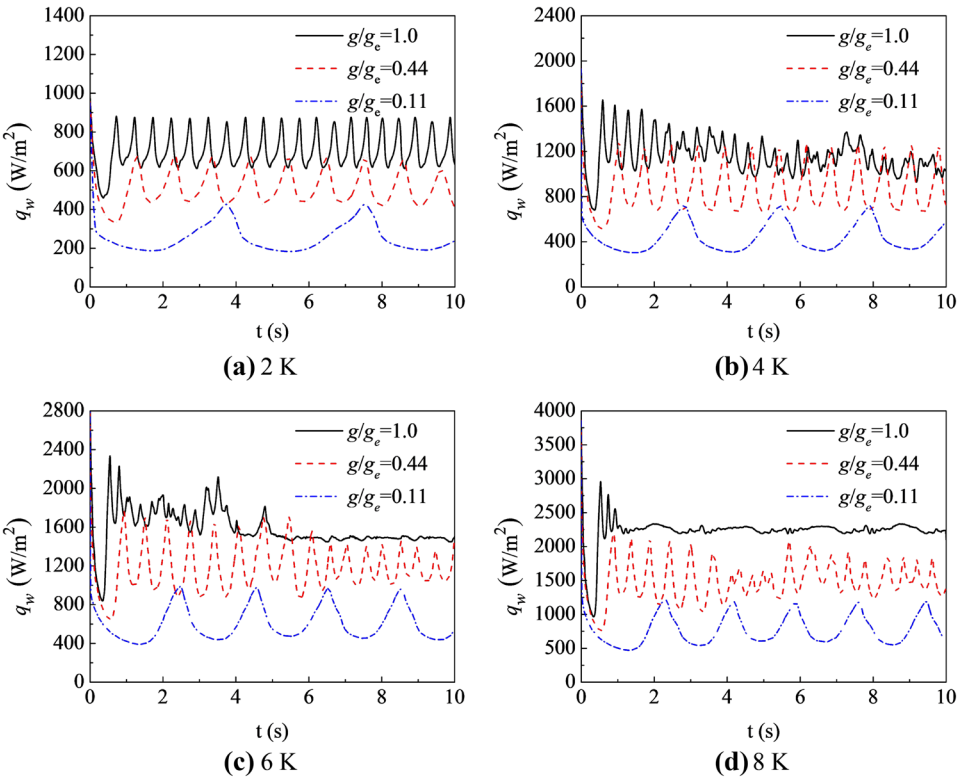

Fig. 13 Influence of wall superheat on the variation of space-averaged heat flux of MNF film boiling without the magnetic field at different gravity conditions

$$e = \frac{\overline{q_w}}{\overline{q_w}\Big|_{2K}} \tag{24}$$

where $\overline{q_w}\Big|_{2K}$ is the space- and time- averaged heat flux when the wall superheat is 2 K.

Figure 14 shows the variation of the space- and time-averaged heat flux and heat flux enhancement ratio with wall superheat under different gravity levels. e represents the enhanced heat flux ratio, which represents the ratio of space- and time-averaged heat flux between other wall superheats and 2 K. It can be clearly seen from Fig. 14a that under all three gravity levels, with the increase of wall superheat, the heat transported from the wall to the fluid increases, and the heat flux increases. In addition, it can be seen from Fig. 14b that the heat flux enhancement ratio increases with the wall superheat, and the heat flux enhancement ratio is almost equal at the same wall superheat.

(b) With the magnetic field

Figure 15 shows the variation of the spatial average heat flux of film boiling with the uniform magnetic field of $H = 20$kA/m. Compared with the results without the magnetic field, the variation of spatial average

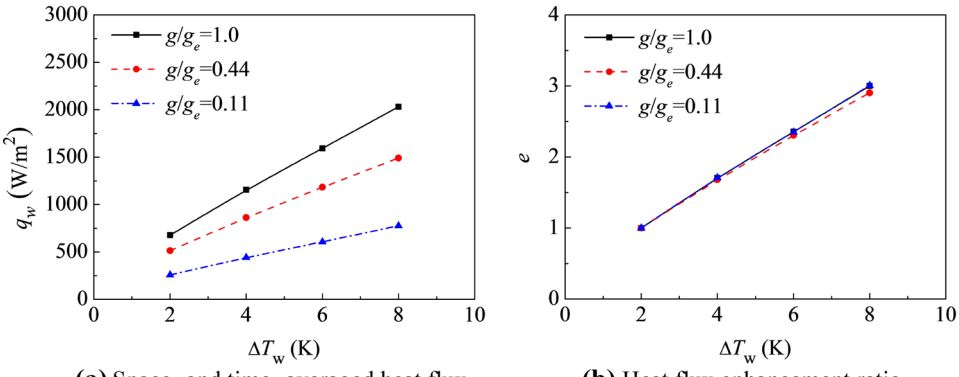

Fig. 14 Influence of wall superheat on heat transfer characteristics without the magnetic field

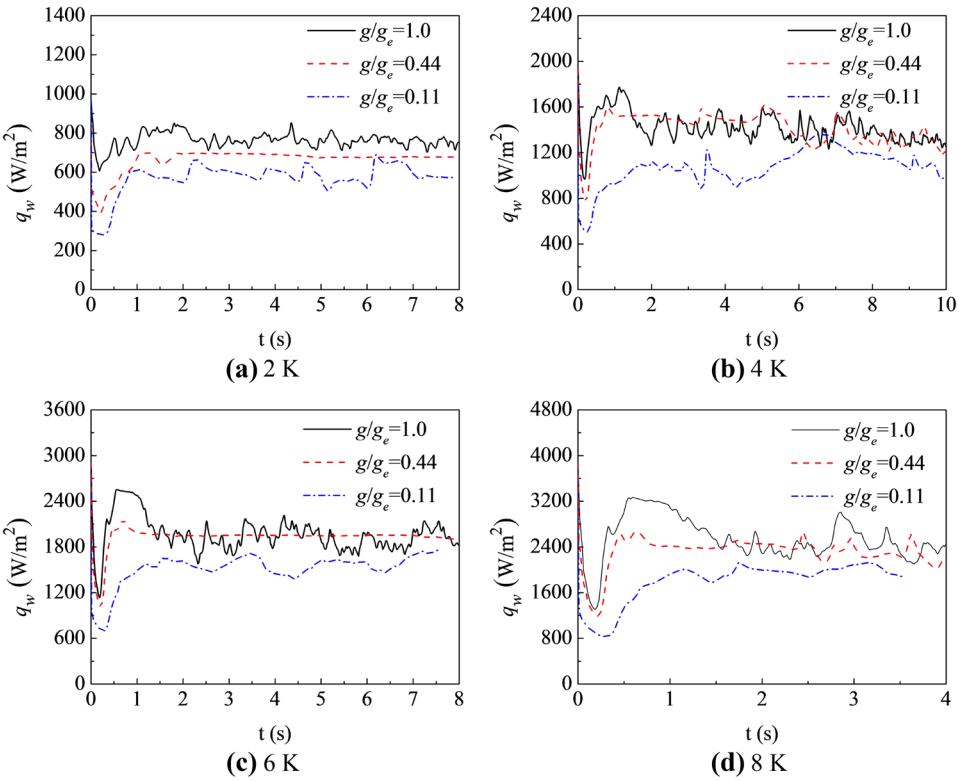

Fig. 15 Influence of wall superheat on the variation of space-averaged heat flux of MNF film boiling with the uniform magnetic field of $H = 20$ kA/m at different gravity conditions

heat flux with time no longer shows periodicity under all three gravity levels after applying the magnetic field, and the distribution of heat flux also reflects the non-periodicity of bubble growth and detachment.

Figure 16 shows the effect of the wall superheat on the space- and time-averaged heat flux and heat flux enhancement ratio of MNF film boiling under different gravity when the vertical magnetic field is applied. As can be seen from Fig. 16a, when the magnetic field is applied, the gap between the space- and time-averaged heat flux under three gravity levels is significantly reduced compared with the case without the magnetic field (see Fig. 14a). This phenomenon caused by the magnetic field had been explained in detail in the author's previous study (Karimi-Moghaddam et al. 2014). As can be seen from Fig. 16b, when the magnetic field is applied, the heat flux enhancement ratios under the three gravity levels are almost equal, which is consistent with the case without the magnetic field (see Fig. 14b).

Table 2 also shows the space- and time-averaged heat flux and heat flux enhancement ratio corresponding to different superheats at different gravity levels. The results show that: (1) After applying the mag-

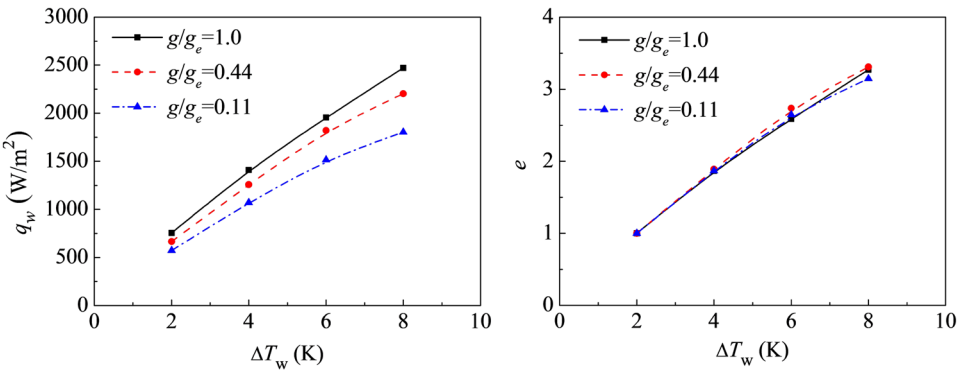

Fig. 16 Influence of wall superheat on heat transfer characteristics with the uniform magnetic field of $H = 20$ kA/m

Table 2 Effect of the wall superheat on heat flux and heat flux enhancement ratio at different gravity levels

H_0 (kA/m)	g/g_e	2 K				4 K				6 K				8 K			
		q_w (W/m^2)	ζ_q (%)	e	ζ_e (%)	q_w (W/m^2)	ζ_q (%)	e	ζ_e (%)	q_w (W/m^2)	ζ_q (%)	e	ζ_e (%)	q_w (W/m^2)	ζ_q (%)	e	ζ_e (%)
0	1.0	677	/	1	/	1154	/	1.7	/	1593	/	2.4	/	2030	/	3.0	/
	0.44	513	/	1	/	862	/	1.7	/	1183	/	2.3	/	1490	/	2.9	/
	0.11	258	/	1	/	441	/	1.7	/	606	/	2.4	/	775	/	3.0	/
20	1.0	755	11.5	1	0	1409	22.1	1.9	9.4	1954	22.7	2.6	10	2470	21.7	3.3	9.1
	0.44	665	29.6	1	0	1257	45.8	1.9	12.5	1820	53.9	2.7	18.7	2202	47.8	3.2	14.1
	0.11	573	122	1	0	1070	142.5	1.9	9.2	1516	150.1	2.7	12.6	1802	132.4	3.2	4.7

netic field, the heat flux increases; (2) With the wall superheat, the heat flux increases; (3) After applying the magnetic field, the heat flux enhancement ratio increases, indicating that the magnetic field enhances the influence of wall superheat on heat transfer characteristics.

In addition, to show the coupling effect of the external magnetic field and wall superheat to enhance heat transfer more clearly, it is necessary to further compare and analyze the heat transfer characteristics in the presence and absence of the magnetic field. Figure 17 shows the comparison of heat transfer characteristics enhanced by the coupling of the magnetic field and wall superheat. ζ_q represents the rate of heat flux enhancement caused by the magnetic field, which can be expressed as follows:

$$\zeta_q = \frac{q_w^{\mathrm{MF}} - q_2^0}{q_2^0} \times 100\% \tag{25}$$

where, the superscript MF represents the magnetic field and 0 represents the non-magnetic field. ζ_e represents the ratio of heat flux enhancement ratio with and without the magnetic field, which can be expressed as follows:

$$\zeta_e \frac{e^{\mathrm{MF}} - e^0}{e^0} \times 100\% \tag{26}$$

It can be seen from Fig. 15a that the magnetic field has a significant enhancement on the heat transfer characteristics, and when the wall superheat is 6 K, the enhancement rate is the highest. Moreover, as the gravity level decreases, the dominant role of buoyancy gradually weakened and the role of magnetic force gradually strengthened so that the enhancement effect of the magnetic field on heat transfer characteristics becomes higher and higher. Under the three gravity levels of $g/g_e = 1.0$, $g/g_e = 0.44$ and $g/g_e = 0.11$, the heat flux can be enhanced up to 22.7%, 53.9% and 150.1%, respectively. From Fig. 17b, it can be more clearly seen that the magnetic field can enhance the enhancement effect of wall superheat on heat transfer characteristics. Similarly, when the wall superheat is 6 K, the enhancement rate is the highest. And, among the three gravity levels studied in this paper, the enhancement rate under $g/g_e = 0.44$ is the highest. Under the three gravity levels of $g/g_e = 1.0$, $g/g_e = 0.44$ and $g/g_e = 0.11$, the heat flux enhancement rate can be enhanced up to 10%, 18.7% and 12.6%, respectively.

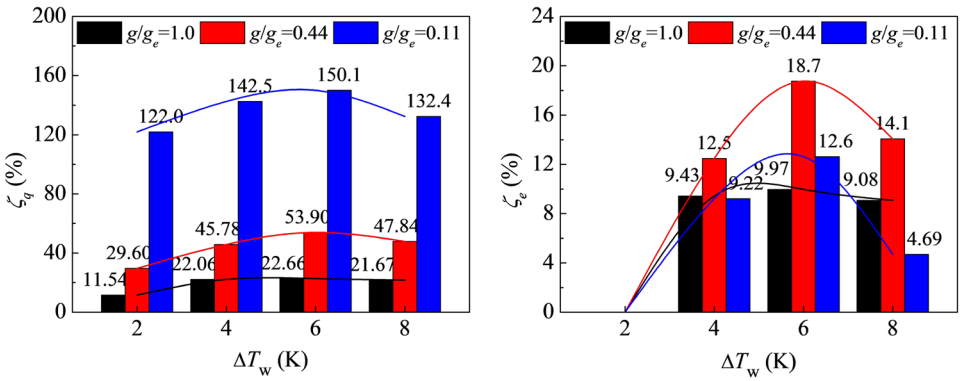

(a) Space- and time- averaged heat flux **(b)** Heat flux enhancement ratio

Fig. 17 Coupling effect of the magnetic field and wall superheat on heat transfer enhancement

Conclusions

The MNF boiling heat transfer under reduced gravity is more complicated than that under the earth's gravity. In this paper, by using the developed computational model of MNF boiling flow, the coupling effect between the magnetic field and wall superheat on MNF boiling thermal dynamics in the reduced gravity is further discussed. The main conclusions are as follows:

1. When the magnetic field is applied, the flow state is no longer periodic. When the superheat is 2 K and 4 K, the flow state is disordered bubble flow, and when the superheat is 6 K ~ 8 K, the flow state is changed to the state of bubble flow and vapor column flow simultaneously. Compared with the results without the magnetic field, the applied magnetic field retards the flow state development of MNF film boiling. Under $g/g_e = 0.44$, the MNF film boiling flow within 2 K ~ 8 K without the magnetic field is in the bubble flow with regular departure. When the magnetic field is applied, the flow state is transformed into a stable and regular vapor column flow. When the gravity level decreases to $g/g_e = 0.11$, the flow state becomes unstable and irregular vapor column flow.
2. Compared with the non-magnetic field, the heat flux is enhanced after applying the magnetic field and the results under different gravity are also discussed. Under the gravity of $g/g_e = 0.11$, the heat flux of 2 K, 4 K, 6 K and 8 K can be enhanced by 122%, 142.5%, 150.1% and 132.4%, respectively.
3. The larger the heat flux enhancement ratio is, the stronger the coupling effect between the magnetic field and wall superheat is. Among the three gravity, the heat flux enhancement ratio under the gravity of $g/g_e = 0.44$ is the largest. Under the gravity of $g/g_e = 0.44$, the heat flux enhancement ratio of 4 K, 6 K and 8 K can be enhanced by 12.5%, 18.7% and 14.1%, respectively.

The results obtained in this paper can provide a more beneficial reference for the design of an enhanced heat transfer scheme of space equipment under reduced gravity.

Authors' Contributions Kaikai Guo and Huixiong Li proposed the conceptualization; Kaikai Guo was responsible for the original draft preparation; Yuan Feng and Tai Wang reviewed and edited the original draft; Jianfu Zhao supervised the research of the paper and gave suggestions for revision. All authors reviewed the manuscript.

Funding The authors acknowledge the support from the joint fund between the Chinese Academy of Sciences (CAS) and National Natural Science Foundation of China (NSFC) under the grant of U1738105.

Availability of Data and Material The authors declare that the data supporting the findings of this study are available within the article.

Declarations

Ethics Approval Not applicable.

Consent to Participate Not applicable.

Consent for Publication All authors have agreed to publish the manuscript.

Conflicts of Interest No competing interests.

References

Abdollahi, A., Salimpour, M.R., Etesami, N.: Experimental analysis of magnetic field effect on the pool boiling heat transfer of a ferrofluid. Appl. Therm. Eng. **111**, 1101–1110 (2017)

Bahiraei, M., Mazaheri, N., Hanooni, M.: Employing a novel crimped-spiral rib inside a triple-tube heat exchanger working with a nanofluid for solar thermal applications: Irreversibility characteristics. Sustainable Energy Technol. Assess. **52** (2022)

Celata, G.P.: Review of flow boiling heat transfer under microgravity conditions. Aust. J. Mech. Eng. **4**(1), 1–13 (2015)

Chang, F., Shang, Y., Hu, H., Li, X., Guo, K., Li, H.: Numerical study on magnetic nanofluid (MNF) film boiling in non-uniform magnetic fields generated by current carrying wires. Int. J. Therm. Sci. **175** (2022)

Dhir, V.K., Warrier, G.R., Aktinol, E., Chao, D., Eggers, J., Sheredy, W., Booth, W.: Nucleate pool boiling experiments (NPBX) on the international space station. Microgravity Sci. Technol. **24**(5), 307–325 (2012)

Guo, K.K., Chang, F.C., Li, H.X.: Application of the magnetic field in Saturated Film Boiling of a Magnetic Nanofluid (MNF) under Reduced Gravity. Energies **14**(3) (2021)

Guo, K.K., Li, H.X., Feng, Y., Wang, T., Zhao, J.F.: Numerical simulation of magnetic nanofluid (MNF) film boiling using the VOSET method in presence of a uniform magnetic field. Int. J. Heat Mass Transf. **134**, 17–29 (2019a)

Guo, K.K., Li, H.X., Feng, Y., Wang, T., Zhao, J.F.: Enhancement of non-uniform magnetic field on saturated film boiling of magnetic nanofluid (MNF). Int. J. Heat Mass Transf. **143**, 12 (2019b)

Hosseinzadeh, K., Montazer, E., Shafii, M.B., Ganji, D.D.: Heat transfer hybrid nanofluid (1-Butanol/MoS2-Fe3O4) through a wavy porous cavity and its optimization. Int. J. Numer. Meth. Heat Fluid Flow **31**(5), 1547–1567 (2021)

Huang, Y.P., Yang, Q., Zhao, J.Q., Miao, J.Y., Shen, X.B., Fu, W.C., Wu, Q., Guo, Y.D.: Experimental Study on Flow Boiling Heat Transfer Characteristics of Ammonia in Microchannels. Microgravity Sci. Technol. **32**(3), 477–492 (2020)

Karimi-Moghaddam, G., Gould, R.D., Bhattacharya, S.: Investigation of enhancement in pool boiling heat transfer of a binary temperature sensitive magnetic fluid, in: ASME International Mechanical Engineering Congress and Exposition (IMECE2013), San Diego, CA (2014)

Kharangate, C.R., Mudawar, I.: Review of computational studies on boiling and condensation. Int. J. Heat Mass Transf. **108**, 1164–1196 (2017)

Kim, S.J., Bang, I.C., Buongiorno, J., Hu, L.W.: Surface wettability change during pool boiling of nanofluids and its effect on critical heat flux. Int. J. Heat Mass Transf. **50**(19–20), 4105–4116 (2007)

Konishi, C., Mudawar, I.: Review of flow boiling and critical heat flux in microgravity. Int. J. Heat Mass Transf. **80**, 469–493 (2015)

Lee, J.H., Lee, T., Jeong, Y.H.: Experimental study on the pool boiling CHF enhancement using magnetite-water nanofluids. Int. J. Heat Mass Transf. **55**(9–10), 2656–2663 (2012)

Ling, K., Son, G., Sun, D.L., Tao, W.Q.: Three dimensional numerical simulation on bubble growth and merger in microchannel boiling flow. Int. J. Therm. Sci. **98**, 135–147 (2015)

Liu, B., Kong, X., Wei, J.J., Zhang, Y.H., Zhao, J.F., Yang, Y.: Pool boiling heat transfer and its critical heat flux mechanism in short-term microgravity. Chinese Science Bulletin-Chinese **65**(17), 1715–1722 (2020)

Ma, X.J., Cheng, P., Gong, S., Quan, X.J.: Mesoscale simulations of saturated pool boiling heat transfer under microgravity conditions. Int. J. Heat Mass Transf. **114**, 453–457 (2017)

Mazaheri, N., Bahiraei, M., Razi, S.: Second law performance of a novel four-layer microchannel heat exchanger operating with nanofluid through a two-phase simulation. Powder Technol. **396**, 673–688 (2022)

Ohta, H., Baba, S.: Boiling Experiments Under Microgravity Conditions. Experimental Heat Transfer **26**(2–3), 266–295 (2013)

Özdemir, M.R., Sadaghiani, A.K., Motezakker, A.R., Parapari, S.S., Park, H.S., Acar, H.Y., Koşar, A.: Experimental studies on ferrofluid pool boiling in the presence of external magnetic force. Appl. Therm. Eng. **139**, 598–608 (2018)

Pandey, V., Biswas, G., Dalal, A.: Saturated film boiling at various gravity levels under the influence of electrohydrodynamic forces. Phys. Fluids **29**(3), 032104 (2017)

Premnath, K.N., Hajabdollahi, F., Welch, S.W.J.: Surfactant effects on interfacial flow and thermal transport processes during phase change in film boiling. Phys. Fluids **30**(4) (2018)

Rosensweig, R.E.: Ferrohydrodynamics. Cambridge University Press, Cambridge (1985)

Rostami, A.K., Hosseinzadeh, K., Ganji, D.D.: Hydrothermal analysis of ethylene glycol nanofluid in a porous enclosure with complex snowflake shaped inner wall. Waves in Random and Complex Media **32**(1), 1–18 (2022)

Sedaghatkish, A., Sadeghiseraji, J., Jamalabadi, M.Y.A.: Numerical simulation of magnetic nanofluid (MNF) film boiling on cylindrical heated magnet using phase field method. Int. J. Heat Mass Transf. **152** (2020)

Sheikholeslami, M., Ebrahimpour, Z.: Thermal improvement of linear Fresnel solar system utilizing Al2O3-water nanofluid and multi-way twisted tape. Int. J. Therm. Sci. **176** (2022)

Sheikholeslami, M., Said, Z., Jafaryar, M.: Hydrothermal analysis for a parabolic solar unit with wavy absorber pipe and nanofluid. Renew. Energy **188** (2022)

Sun, D.L., Qu, Z.G., He, Y.L., Tao, W.Q.: An efficient segregated algorithm for incompressible fluid flow and heat transfer problems—IDEAL (Inner Doubly Iterative Efficient Algorithm For Linked Equations) Part I: Mathematical formulation and solution procedure. Numerical Heat Transfer, Part B: Fundamentals **53**(1), 1–17 (2008)

Sun, D.L., Tao, W.Q.: A coupled volume-of-fluid and level set (VOSET) method for computing incompressible two-phase flows. Int. J. Heat Mass Transf. **53**(4), 645–655 (2010)

Udaykumar, H.S., Mittal, R., Shyy, W.: Computation of solid–liquid phase fronts in the sharp interface limit on fixed grids. J. Comput. Phys. **153**, 535–574 (1999)

Wan, S.X., Zhao, J.F.: Pool boiling in microgravity: Recent results and perspectives for the project DEPA-SJ10. Microgravity Sci. Technol. **20**(3–4), 219–224 (2008)

Xue, Y.F., Zhao, J.F., Wei, J.J., Li, J., Guo, D., Wan, S.X.: Experimental study of nucleate pool boiling of FC-72 on smooth surface under microgravity. Microgravity Sci. Technol. **23**, S75–S85 (2011)

Zhao, J.F., Li, Z.D., Zhang, L., Li, J.C., Fu, S.: Numerical simulation of single bubble pool boiling in different gravity conditions. AIP Conf. Proc. **1376**, 565–568 (2011)

Zhu, C.-S., Hu, Z., Wang, K.-M.: Multi-bubble motion behavior of uniform magnetic field based on phase field model. Chin. Phys. B **29**(3) (2020)